MOLECULAR AND CELLULAR BIOLOGY, Jan. 2005, p. 294–302 Vol. 25, No. 1
0270-7306/05/$08.00+0 doi:10.1128/MCB.25.1.294–302.2005

Generation and Characterization of Endonuclease G Null Mice†

Ryan A. Irvine,[1] Noritaka Adachi,[1] Darryl K. Shibata,[1] Geoffrey D. Cassell,[1] Kefei Yu,[1] Zarir E. Karanjawala,[1] Chih-Lin Hsieh,[2] and Michael R. Lieber[1]*

Departments of Pathology, of Biochemistry & Molecular Biology, of Molecular Microbiology & Immunology, and of Biological Sciences[1] and Departments of Urology and of Biochemistry & Molecular Biology,[2] Norris Comprehensive Cancer Center, Keck School of Medicine, University of Southern California, Los Angeles, California

Received 19 August 2004/Returned for modification 24 September 2004/Accepted 10 October 2004

Endonuclease G (endo G) is one of the most abundant nucleases in eukaryotic cells. It is encoded in the nucleus and imported to the mitochondrial intermembrane space. This nuclease is active on single- and double-stranded DNA. We genetically disrupted the *endo G* gene in mice without disturbing a conserved, overlapping gene of unknown function that is oriented tail to tail with the *endo G* gene. In these mice, the production of endo G protein is not detected, and the disruption abolishes the nuclease activity of endo G. The absence of endo G has no effect on mitochondrial DNA copy number, structure, or mutation rate over the first five generations. There is also no obvious effect on nuclear DNA degradation in standard apoptosis assays. The endo G null mice are viable and show no age-related or generational abnormalities anatomically or histologically. We infer that this highly conserved protein has no mitochondrial or apoptosis function that can discerned by the assays described here and that it may have a function yet to be determined. The early embryonic lethality of *endo G* null mice recently reported by others may be due to the disruption of the gene that overlaps the *endo G* gene.

Endonuclease G (endo G) is the most abundant and active nuclease in all eukaryotic mitochondria and one of the most abundant nucleases in whole-cell extracts from eukaryotic cells. The function of endo G has been a matter of considerable uncertainty. It is expressed ubiquitously in all eukaryotes, and the gene is highly conserved in organisms ranging from *Saccharomyces cerevisiae* to humans (8, 19, 20). endo G is located primarily or exclusively in the mitochondrial intermembrane space (8), except during cell death, at which time it can be released along with other proapoptotic proteins (15, 18, 28).

endo G has been considered a candidate for processing primers for mitochondrial DNA (mtDNA) replication (8). RNA-DNA hybrids in the form of R-loops are known to be generated at eukaryotic mitochondrial conserved sequence blocks during transcription (4–6, 14, 23, 24). The RNA in these R-loops was thought to serve as a primer for mtDNA replication (7, 8). However, other nucleases, specifically MRP (RNase mitochondrial RNA processing) or RNase H, might also serve that role (3, 13, 14).

More recently, studies have reported a possible role for endo G as one of the apoptotic nucleases in multicellular eukaryotes (15, 18). The primary eukaryotic apoptotic nuclease is DFF (DNA fragmentation factor), which is also called CAD (caspase-activated DNase) or CPAN (caspase-activated nuclease) in the literature. DFF is a dimer of DFF40 and DFF45. Residual DNA degradation in DFF45 null mice suggests that other nucleases may be involved in apoptosis, and genetic studies of *Caenorhabditis elegans* and biochemical studies of mammalian cells suggest that endo G may be one of the nucleases involved in apoptosis (15, 18).

Our interest in endo G arose because of its high efficiency in cleaving the DNA strands in an R-loop (R. B. West, J. Courcelle, and M. R. Lieber, unpublished data). We were interested in R-loops because of their role in immunoglobulin class switch recombination (26). We fractionated lymphoid cell extracts, and on the basis of immunoblotting and enzymatic characterization, the peak R-loop cutting activity turned out to be endo G (R. B. West and M. R. Lieber, unpublished data). Because of the mitochondrial intermembrane space location of endo G, we were skeptical that it played any role in class switch recombination. However, given the very high rate of enzymatic action by endo G on R-loops, we could not rule out the possibility of small amounts of endo G being processed into a nuclear form or being exported from the mitochondria in B cells. Indeed, endo G was originally described as a scarce nuclear protein (7, 10). Hence, the only way to formally test for a role of endo G in class switch recombination was to genetically knock it out and then analyze class switching, in addition to analyzing apoptosis and mtDNA. We report our results here. After we had completed this study and were preparing the manuscript for publication, another group reported a very different phenotype for *endo G* null mice (28). The likely basis for this disparity is that we eliminated expression of only the *endo G* gene, and the other group inadvertently deleted half of a gene immediately adjacent to the *endo G* gene in addition to the *endo G* gene.

MATERIALS AND METHODS

Construction of the murine *endo G* targeting vector and selection of embryonic stem (ES) cell homologous recombinants. The targeting vector pNA2 was constructed with a mouse phosphoglycerate kinase 1 (*PGK*) neomycin (neo) expres-

* Corresponding author. Mailing address: Norris Comprehensive Cancer Center, Rm. 5428, Keck School of Medicine, University of Southern California, 1441 Eastlake Ave., MC9176, Los Angeles, CA 90033. Phone: (323) 865-0568. Fax: (323) 865-0570. E-mail: lieber@usc.edu.

† Supplemental material for this article may be found at http://mcb.asm.org/.

sion cassette separating two blocks of *endo G* homologous sequence (Fig. 1A). Homology block A, which comprises exon 1 and most of intron 1 of the *endo G* gene, was amplified from mouse genomic DNA using primers 1 and 2 (Table 1). The 1.5-kb PCR fragment was digested with BsrGI and NsiI and then ligated into the reciprocal sites of pBSDT, a plasmid derived from pBluescript (Stratagene, La Jolla, Calif.) containing a diphtheria toxin (DT) expression cassette. Homology block B, which comprises intron 2 and exon 3 of the *endo G* gene as well as exons 10, 11, and 12 of an overlapping gene of unknown function (i.e., D2Wsu81; locus identification number 227695), was amplified using primers 3 and 4 (Table 1). The 2.8-kb PCR fragment was digested with SalI and ligated into the SalI site of block A-containing pBSDT. Finally, a 2.2-kb HindIII fragment from vector pXW4 that contained a *PGK*neo expression cassette was blunted with Klenow DNA polymerase and ligated into the EcoRV site of block A- and block B-containing pBSDT, creating targeting vector pNA2. W9.5 ES cells, derived from the 129/SvJ mouse strain, were electroporated with AhdI-linearized pNA2 and subjected to G418 selection by Xenogen Genetics (St. Louis, Mo.). Of the 192 G418-resistant clones screened for the targeted *endo G* locus by PCR (using primers 1 and 5 [Table 1]), only clone 169 was positive for the 1.6-kp fragment.

***endo G* mutant mice.** After targeted recombination was confirmed by Southern blot analysis using a 1-kb *endo G* 3′ probe (PCR amplified using primers 6 and 7 [Table 1]), C57BL/6J donor blastocysts were injected with recombinant ES cells expanded from clone 169 (injection took place at the Norris Cancer Center Transgenic Core Facility of the University of Southern California in Los Angeles). Heterologous blastocysts were then transferred to pseudopregnant DBA/2 female mice, and chimeric offspring were identified by coat color. Two chimeric males demonstrated germ line transmission of the targeted *endo G* locus through matings with C57BL/6J females. Mice heterozygous for the *endo G* mutant allele were identified by PCR (using primers 1 and 5 [Table 1]) and confirmed by genomic Southern blot analysis of tail DNA (Fig. 1B and C). Homozygous mice were produced by crossing heterozygous animals and identified by PCR and Southern blot analysis as described below. For the routine screening of animals in which the *endo G* gene had been genetically disrupted (knockout [KO]), the absence of a wild-type (WT) *endo G* allele was determined by PCR using primers 8 and 9 (Table 1 and Fig. 1A and B).

Western blot analysis. Whole-cell kidney extracts were prepared from 3-month-old WT and *endo G* KO mice as follows. Minced kidney tissue was Dounce homogenized in cold radioimmunoprecipitation assay (RIPA) buffer (10 mM sodium phosphate [pH 7.2], 2 mM EDTA, 150 mM NaCl, 50 mM NaF, 0.2 mM Na_3OV_4, 1% sodium deoxycholate, 1% Nonidet P-40, 0.1% sodium dodecyl sulfate [SDS]) supplemented with leupeptin (2 μg/ml) and aprotinin (2 μg/ml). The homogenate was sonicated three times for 30 s each time using a Branson sonifier 450 equipped with a microtip (4.5 output; 70% duty cycle). The lysate was centrifuged at 100,000 × *g* for 1 h at 4°C in a Beckman Optima TL ultracentrifuge. The total protein concentration of the supernatant (i.e., the whole-cell extract) was estimated by the Bradford method using the Bio-Rad (Hercules, Calif.) protein assay reagent. The extract was boiled in an equal volume of 4× Laemmli buffer and 60 μg of total protein was separated on an SDS-10% polyacrylamide gel. Proteins were transferred to Immobilon-P^{sq} 0.2-μm-pore-size polyvinylidene difluoride membrane (Millipore, Bedford, Mass.) and blotted with a 1:1,000 dilution of affinity-purified, rabbit anti-mouse endo G polyclonal immunoglobulin G (IgG) (a gift from A. Ruiz-Carrillo, Laval University School of Medicine, Ste. Foy, Quebec, Canada). Immunopositive bands were visualized using a 1:3,000 dilution of goat anti-rabbit IgG conjugated to horseradish peroxidase (HRP) (Bio-Rad) and the Pierce (Rockford, Ill.) SuperSignal West Pico chemiluminescence detection kit. Western blots of purified Myc-labeled endo G proteins were developed using 1:10,000 dilutions of mouse monoclonal IgG MCY1-9E10.2 (ATCC CRL 1729) and HRP-conjugated goat anti-mouse IgG (Bio-Rad).

Preparation of Myc-tagged endo G proteins and the R-loop cutting assay. The full-length endo G expression vector, pRI-3, was constructed by inserting a 2.4-kb, BamHI/BstBI-digested PCR fragment (amplified from mouse genomic DNA using primers 10 and 11 [Table 1]), comprising the entire *endo G* coding sequence, into the reciprocal sites of vector pcDNA6/*myc*-His (Invitrogen, Carlsbad, Calif.). The *endo G* exon 2-minus (ΔE2) expression vector, pRI-5, was constructed by inserting a 0.5-kb, BamHI/BstBI-digested PCR fragment (amplified from mouse genomic DNA using primers 10 and 12 [Table 1]), comprising exon 1 of the *endo G* gene and the 9-nucleotide (nt) exon 3 alternate open reading frame (ORF) (carried on primer 12), into the reciprocal sites of vector pcDNA6/*myc*-His.

By using the calcium phosphate method, 293/EBNA1 cells (10a) grown to 30% confluence in Dulbecco modified Eagle medium that contained 10% fetal bovine serum (FBS), penicillin (100 U/ml), and streptomycin sulfate (100 μg/ml) were transfected with 30 μg of plasmid DNA per 15-cm-diameter dish. After 48 h, cells were pelleted by centrifugation, washed in cold phosphate-buffered saline (PBS), and resuspended in 10 ml of lysis buffer (25 mM HEPES [pH 7.9], 5 mM $MgCl_2$, 150 mM NaCl, 0.1% Nonidet P-40, 1 mM dithiothreitol [DTT]) that contained aprotinin (1 μg/ml), leupeptin (1 μg/ml), pepstatin A (1 μg/ml), and phenylmethylsulfonyl fluoride (PMSF) (0.2 mM). The cell suspension was sonicated four times for 30 s each time (2 output; 70% duty cycle), and the resulting lysate was centrifuged at 30,000 × *g* for 1 h at 4°C. The cell extract was precleared with protein G-Sepharose (50% slurry in PBS) for 30 min at room temperature (RT) with rotary mixing. Myc-tagged endo G proteins were immunoprecipitated with mouse monoclonal IgG MCY1-9E10.2 (25 μg/ml) in the presence of 25 μl of protein G-Sepharose slurry per ml for 1 h at RT with mixing as described above. The antibody-bound Sepharose beads were washed sequentially with the following buffers (washed in each buffer for 5 min) at RT: lysis buffer, immunoprecipitation (IP) wash buffer (25 mM HEPES [pH 7.9], 10 mM $MgCl_2$, 650 mM KCl, 0.1% Nonidet P-40), and PBS. The Sepharose beads were resuspended in an equal volume of PBS, creating a 50% slurry, and stored on ice until use.

To measure the activity of the Myc-tagged endo G proteins, 2.5 μl of protein-bound Sepharose bead slurry was mixed with 10 ng of plasmid pTW-SS22 that had been transcribed with T7 RNA polymerase or that had not been transcribed with T7 polymerase. The plasmid pTW-SS22 contains 12.5 murine Sγ3 immunoglobulin class switch repeats cloned into the multicloning site (25). The reaction (20-μl reaction mixture) was performed in endo G reaction buffer (20 mM Tris-Cl [pH 8.0], 50 mM KCl, 4 mM $MgCl_2$, 1 mM DTT, 2 mM ATP, 0.05% bovine serum albumin [BSA] [17]) for 30 min at 37°C. The DNA was phenol and chloroform extracted, ethanol precipitated, and then digested with XmnI. The entire sample was electrophoresed through a 0.8% LE agarose gel, transferred to a 0.45-μm-pore-size nylon membrane (GE Osmonics, Minnetonka, Minn.), and probed with BamHI-linearized, ^{32}P-labeled pTW-SS22. The blot was exposed to a phosphor screen (Kodak, Rochester, N.Y.) and visualized using a Bio-Rad Molecular Imager FX.

Total cellular DNA purification and mtDNA Southern blots. Total cellular DNA was purified from 300 mg of freshly dissected and minced mouse liver tissue as follows. The tissue was washed in PBS, snap-frozen in liquid nitrogen, and pulverized with a Teflon pestle. The ground tissue was suspended in 6 ml of TE (50 mM Tris-Cl [pH 8.0], 10 mM EDTA) supplemented with proteinase K (1 mg/ml) and SDS (0.5%). The suspension was incubated at 50°C for 3 h with frequent mixing by inversion. RNase A (20 μg/ml) was then added, and the mixture was incubated for an additional hour at 50°C. The lysate was centrifuged at 35,000 × *g* for 15 min at 4°C. The cleared lysate was phenol and chloroform extracted, and the DNA was ethanol precipitated. The DNA pellet was dissolved in TE (pH 8.0) and quantified using a Bio-Rad Versafluor fluorometer and the Bio-Rad fluorescent DNA quantitation kit according to the manufacturer's protocol.

About 400 ng of total mouse liver DNA was digested for 16 h at 37°C with NsiI, EcoRV, or BglII/EcoRI. Digests were electrophoresed through a 0.8% LE agarose gel and transferred to a 0.45-μm-pore-size nylon membrane. The membrane was probed with a mixture of three EcoRV-digested, ^{32}P-labeled plasmids, MumX-1.9, -5.1, and -7.6, each of which contains a unique XbaI fragment of murine mtDNA (a gift from G. Attardi, California Institute of Technology, Pasadena). The blot was visualized as described above.

Sequencing of the murine mtDNA DLR. To purify mtDNA for sequencing, a modified version of the Michikawa and Attardi protocol (16) was used. Briefly, 25 μg of total cellular DNA from mouse liver (see above) were digested with 20 U each of NotI and DraIII (New England Biolabs, Beverly, Mass.) for 2 h at 37°C. Next, 100 U of exonuclease III (Roche, Indianapolis, Ind.) were added to the digest, which was incubated for another 2 h at 37°C. The digest was phenol and chloroform extracted, the DNA was ethanol precipitated, and the DNA pellet was dissolved in 100 μl of TE (pH 8.0). With primers 13 and 14 (Table 1), a 700-bp fragment of the murine mtDNA displacement loop region (DLR), encompassing all of the initiation sites for transcription and the primary and secondary origins of heavy-strand DNA synthesis, was amplified in four separate 25-μl reaction mixtures (1 μl of mtDNA template per reaction mixture) using the Roche GC-rich PCR system. The PCR mixtures were mixed, and the DLR PCR fragment was gel purified before being cloned into the pCR2.1-TOPO vector (Invitrogen) in order to screen the bacteria for blue or white color. Individual clones were sequenced using the M13 forward (−20) or reverse primer and a Li-Cor (Lincoln, Nebr.) IR^2 sequencer. For each clone, 350 bp was sequenced from the D-loop, through the conserved sequence boxes (CSBs), to the light-strand promoter LSP (corresponding to nt 15862 to 16212 on the mouse L-cell mtDNA sequence sequenced by Bibb et al. [2]). Mutations were identified as deviations from the mouse L-cell mtDNA sequence sequenced by Bibb et al. (2).

DNA fragmentation and chromatin condensation analyses. Splenocytes were prepared from 10- to 12-week-old WT and KO mice and treated essentially as

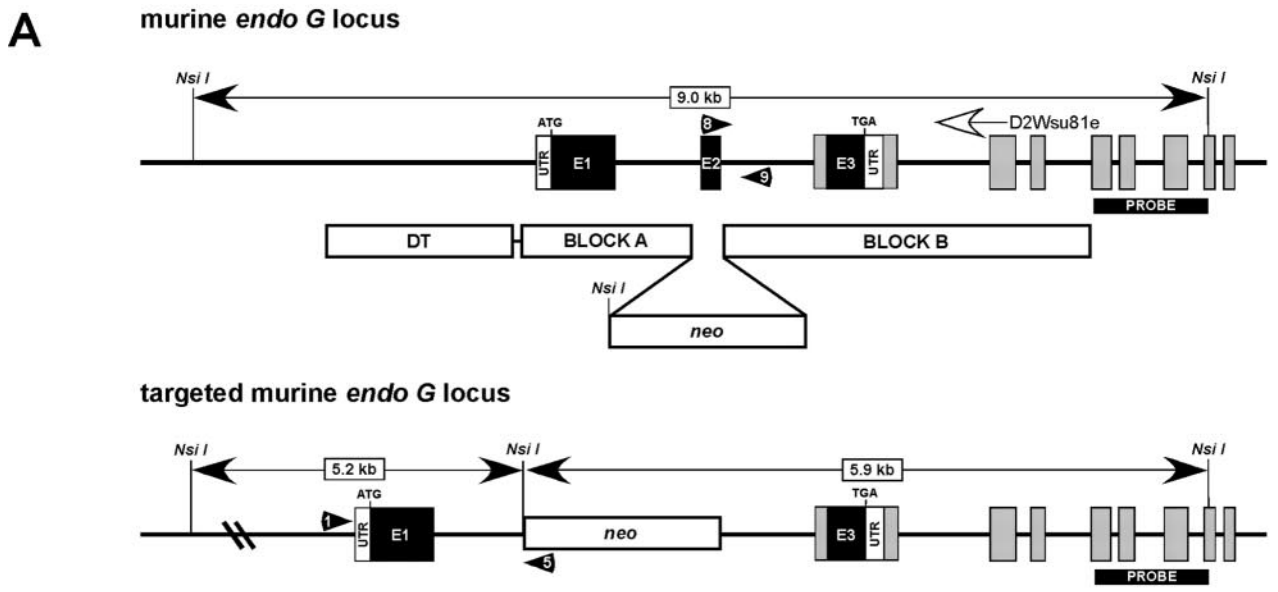
A
murine endo G locus
Nsi I
9.0 kb
Nsi I
ATG
TGA
D2Wsu81e
UTR
E1
E2
E3
UTR
PROBE
DT
BLOCK A
BLOCK B
Nsi I
neo
targeted murine endo G locus
Nsi I
5.2 kb
Nsi I
5.9 kb
Nsi I
ATG
TGA
UTR
E1
neo
E3
UTR
PROBE

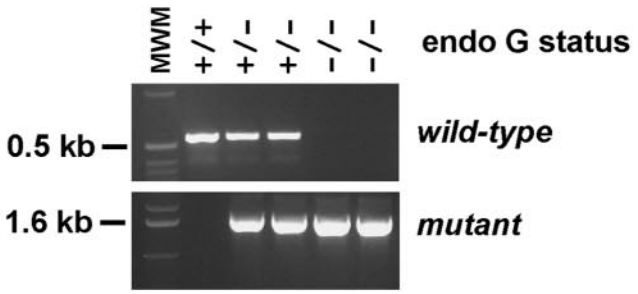
B
MWM
+/+
+/-
+/-
-/-
-/-
endo G status
0.5 kb
wild-type
1.6 kb
mutant

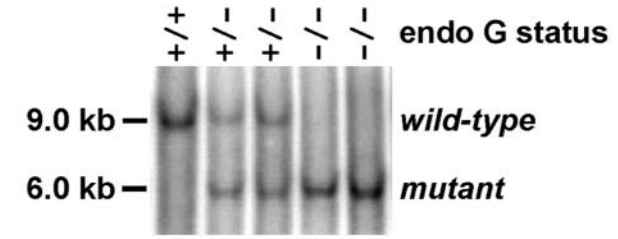
C
+/+
+/-
+/-
-/-
-/-
endo G status
9.0 kb
wild-type
6.0 kb
mutant

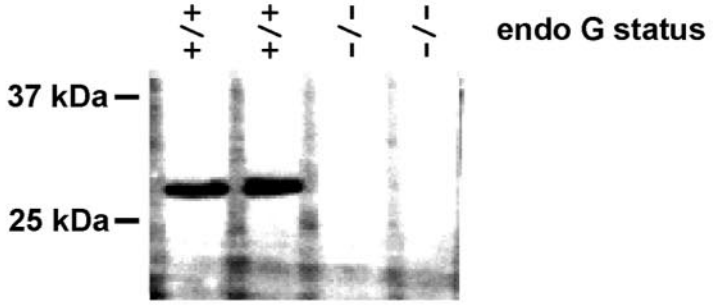
D
+/+
+/+
-/-
-/-
endo G status
37 kDa
25 kDa

described previously (29). Freshly dissected whole spleens were ground through a Cellector tissue sieve (E-C Apparatus Corp., Holbrook, N.Y.) into RPMI 1640 medium that contained 10% FBS and 50 μM 2-mercaptoethanol. After centrifugation at 500 × *g* for 5 min at 4°C and aspiration of the medium, the cell pellet was resuspended in 10 ml of ACK lysis buffer (0.15 M NH_4Cl, 10 mM $KHCO_3$, 0.1 mM EDTA [pH 7.2]) and incubated for 10 min at RT. After centrifugation as described above, splenocytes were washed twice with 10 ml of ice-cold PBS (pH 7.2) that contained 0.5% BSA. Splenocytes were resuspended in RPMI 1640 medium containing 10% FBS and 50 μM 2-mercaptoethanol, 50 μM etoposide (Sigma, St. Louis, Mo.), or 500 nM actinomycin D (Sigma) to a density of 0.5×10^6 cells/ml. For each treatment, 12 ml of cells (6×10^6 cells) were transferred to a single 10-cm-diameter dish and incubated for 12 h at 37°C and 5% CO_2.

Genomic DNA was purified from 5×10^6 cells by standard methods. Briefly, the cell pellet was resuspended in 100 μl of TE to which 1 ml of extraction buffer (10 mM Tris-Cl [pH 8.0], 0.1 M EDTA, 0.5% SDS, 20 μg of DNase-free RNase per ml) was added with gentle mixing by inversion. After incubation for 1 h at 37°C, proteinase K (100 μg/ml) was added, and the lysate was incubated at 50°C for 3 h with occasional mixing as described above. The digest was phenol and chloroform extracted, the DNA was ethanol precipitated, and the DNA pellet was dissolved in 30 μl of TE. Finally, 2 μl of each DNA sample was separated on a 1.5% LE agarose gel.

To visualize nuclear chromatin condensation, 10^6 cells from these dishes were fixed in 3.7% formaldehyde (in PBS) for 10 min at RT, washed twice with 10 ml of Tris-buffered saline (pH 7.2), and stained with 1 μg of 4′, 6-diamidino-2-phenylindole (DAPI) per ml. Nuclear chromatin was visualized with an Olympus AX70 fluorescence microscope equipped with a Spot charge-coupled device camera (Diagnostic Instruments, Inc., Sterling Heights, Mich.). A minimum of 200 nuclei was analyzed for chromatin condensation per treatment arm of the experiment.

Anti-IgM and anti-IgG ELISA. The wells of a 96-well enzyme-linked immunosorbent assay (ELISA) plate were coated for 12 h at 4°C with goat anti-mouse IgG (kappa chain) (Caltag, Burlingame, Calif.) diluted to 1 μg/ml in 0.1 M sodium bicarbonate buffer (pH 9.6). The plate was washed four times (200 μl/well) with PBS that contained 0.05% Tween 20 (PBST). The plate was then blocked for 1 h at RT with RPMI 1640 containing 10% FBS and washed with PBST as described above. Serum samples obtained from 6-week-old WT, *endo G* heterozygous, and *endo G* KO mice were serially diluted in RPMI 1640 containing 10% FBS and transferred to the ELISA plate. After 2-h incubation at RT, the plate was washed with PBST, and then biotinylated anti-mouse IgM (Sigma) (diluted 1:20,000 in RPMI 1640 containing10% FBS) or biotinylated anti-mouse IgG (Pharmacia) (diluted 1:5,000 in RPMI 1640 containing 10% FBS) was added (100 μl/well). After a 2-h incubation at RT, the plate was washed with PBST before streptavidin-conjugated HRP (Pharmacia) (diluted 1:5,000 in PBS) was added (100 μl/well). After 30-min incubation at RT, the plate was washed with PBST and developed using the tetramethyl benzidine substrate reagent set (BD Biosciences Pharmingen, San Diego, Calif.) according to the manufacturer's protocol. The optical density at 450 nm was measured using a Molecular Devices Emax microplate reader.

RESULTS

Generation of *endo* $G^{+/-}$ and *endo* $G^{-/-}$ mice. As described in Materials and Methods, the *endo G* targeting vector, pNA2, was constructed with a mouse phosphoglycerate kinase 1 (*PGK*) neomycin (neo) expression cassette separating two blocks of *endo G* homologous sequence (Fig. 1A). Homology block A comprises exon 1 and most of intron 1 of the *endo G* gene. Homology block B comprises intron 2 and exon 3 of *endo G* as well as exons 10, 11, and 12 of an overlapping gene of unknown function (i.e., D2Wsu81e; locus identification number 227695). W9.5 ES cells were electroporated with AhdI-linearized pNA2 and subjected to G418 selection. G418-resistant clones were screened for the targeted *endo G* locus, and this clone was used to inject blastocysts. Chimeric mice were bred with C57Bl/6J mice with successful germ line transmission to yield *endo*$^+$ or *endo*$^-$ mice. Heterozygous mice yielded litters with the expected ratios of *endo G* genotypes, including the null mutation, *endo* $G^{-/-}$. Upstream and downstream PCR boundaries gave the expected products (verified by sequencing) (Fig. 1B). Southern blot analysis (Fig. 1C) showed a genomic configuration of the disrupted allele that confirmed the organization in Fig. 1A.

Western blot analysis to document the absence of endo G protein. Whole-cell kidney extracts were prepared from 3-month-old WT and *endo* $G^{-/-}$ mice (see Materials and Methods). Western blots were done using a polyclonal antibody that was specific for murine endo G protein. Ample protein at approximately 28 kDa, the position of the mature protein, could be detected in WT samples, but no immunoreactive band could be detected in the samples from *endo* $G^{-/-}$ mice (Fig. 1D). The gels were run with particular attention for immunoreactive bands at faster-migrating positions (as small as 6 kDa), and immunoreactive material was not detected. On the basis of dilutions of the WT samples, we estimate that any residual protein, if present at all, is reduced at least 100-fold in the null cells.

Test of putative truncated protein for nuclease activity. Even though we did not detect any immunoreactive truncated endo G protein from the disrupted allele, we considered the possibility that nondetected amounts of it might be made from exon 1. We further considered the possibility that the exon 1-encoded portion (120 amino acids ↑) of the endo G protein would have any residual nuclease activity. To this end, an *endo G* exon 2-minus (ΔE2) expression vector, pRI-5, was constructed by inserting a 0.5-kb, BamHI/BstBI-digested fragment (verified by sequencing), comprising exon 1 of *endo G* and the 9-nt exon 3 alternate ORF, into pcDNA6/*myc*-His. The corresponding full-length endo G construction was made in parallel; the N-terminal targeting sequence was not included for either form. The full-length and truncated recombinant proteins were produced in human 293 cells, and the proteins were purified

FIG. 1. Disruption of the murine *endo G* gene and characterization of expression. A. *endo G* genomic locus. The murine *endo G* locus is shown on the top line. The blocks of homology used for exchanging exon 2 and replacing it with the *neo* gene are shown below the *endo G* locus map. The configuration of the disrupted (targeted) locus is shown in the third line. The positions of the diphtheria toxin gene (DT), untranslated region (UTR), and primer sites (black arrowheads with white numbers) are indicated. The gene that overlaps with the *endo G* locus is D2Wsu81e and is shown shaded; the most downstream exon of this gene overlaps with all of *endo G* exon 3. B. PCR assay for the wild-type (*endo* $G^{+/+}$ [+/+]) and genetically disrupted alleles (*endo* $G^{+/-}$ [+/−] and *endo* $G^{-/-}$ [−/−]). Primers 8 and 9 are used to identify the wild-type allele, and these primers generate a 530-bp product (Table 1). Primers 1 and 5 (Table 1) are used to detect the disrupted (mutant or KO) allele, and these primers generate a band of approximately 1.6 kb. The positions of molecular size standards (MWM) (in kilobases) are indicated to the left of the gels. C. Southern blot analysis of the wild-type and disrupted allele. The probe indicated in Fig. 1A was used to hybridize to genomic DNA resolved after NsiI digestion. The wild-type allele yields a band of 9 kb, and the disrupted allele yields a band of 5.9 kb. D. Western blot analysis of endo G production in wild-type and null mice. A polyclonal antibody was used to develop a Western blot to reveal the 28-kDa mature form of endo G. No immunoreactive band was detected down to approximately 6 kDa on this and other replicate Western blots.

TABLE 1. PCR primers used in this study

Primer	Sequence
1	5′-GGTCTGACAGATCTGGGGTTCTGTCCTG-3′
2	5′-GGGTCCATGCATGGAGCACACCTCGGACCTTCCATTAG-3′
3	5′-GACGCGTCGACGTAAGCCTGTAGCTGACGGGGC-3′
4	5′-GACGCGTCGACCACCAAAGCTGGTCTCTACTG-3′
5	5′-GGTCCCTCGAATCAAGCTATCGAATTCCTG-3′
6	5′-AGGGAATTCAGCTCTTACTGAGGCAAGAGG-3′
7	5′-ATGCATTCCTCCCTAGGTACCTGAGAAAGG-3′
8	5′-CAGCTTGACGCGAACTTACC-3′
9	5′-CTCACGTGACTGTAACCTG-3′
10	5′-ACTGGATCCACCATGCGCGCGCTGCGGGCCGGCCTGACCCTAGC-3′
11	5′-GTAGCTTTCGAACTTGCTGCCAGCAGTGATAGCCTTGAGG-3′
12	5′-GTAGCTTTCGAAGCCTCGGTCCTGAGGCGCTACGTTGCTCAGGTAGAAG-3′
13	5′-AGACATCTCGATGGTATCG-3′
14	5′-TTTATCACTGCTGAGTCCCGTG-3′

using the C-terminal histidine-tagged myc (his-myc) epitope (Fig. 2A).

Although endo G has a wide spectrum of nuclease activities (double-stranded DNA [dsDNA], single-stranded DNA [ssDNA], ssRNA, and RNA-DNA) (7, 8, 10, 11, 17), it is distinctive for its rapid cleavage of the two DNA strands of an R-loop structure (17) (West et al., unpublished). The cleavage is quite consistent with nicking of the two DNA strands independently at sufficient numbers of locations resulting in a double-strand DNA break (17) (West et al., unpublished). In our experience, endo G is at least 100-fold more active on the displaced single-strand portion of the R-loop relative to dsDNA (West et al., unpublished). This high level of activity provides for a very sensitive assay for small amounts of endo G activity. Therefore, we generated long R-loops at the murine Sγ3 immunoglobulin class switch sequences on a plasmid in vitro (Fig. 2B), as described previously (9, 25). We then incubated the recombinant full-length endo G or the truncated form with the R-loop to permit it to generate nicks and ultimately dsDNA breaks anywhere throughout the 613-bp murine Sγ3 switch region (see Materials and Methods). We then linearized the plasmid at XmnI. Breaks due to endo G anywhere within the R-loop switch region will generate a distribution of linear products between 1726 and 2382 bp and another distribution between 850 and 1506 bp.

We find that the full-length endo G is quite active in cleaving the R-loop structures (Fig. 2C, left gel, FL lane). In contrast, the truncated form of endo G showed no activity on the R-loop (Fig. 2C, left gel, ΔE2 lane). Even intense overexposure of this gel showed no evidence of even minimal R-loop cleavage activity or dsDNA nicking activity by the truncated form. On nontranscribed plasmid, the recombinant full-length endo G has a low but clear dsDNA nicking activity (Fig. 2C, right gel, FL lane), indicated by the smear of products extending down from the 3.2-kb linear band. In contrast, the truncated form also lacks this activity (Fig. 2C, right gel, ΔE2 lane). Therefore, the ΔE2 truncation eliminates all nuclease activity.

Morphological characterization of the mice. Physical examination and gross anatomic dissection of the *endo* $G^{+/-}$ and *endo* $G^{-/-}$ mice did not reveal any abnormalities relative to their wild-type littermates at any age from birth to 1 year of age. Detailed histological analysis of liver, brain, heart, lungs, stomach, small intestine, large intestine, spleen, bone marrow, lymph nodes, skin, eyes, and bone failed to reveal any differences from the wild-type mice at any age. Electron microscopy of liver revealed no ultrastructural cellular differences from the wild-type mouse liver. Examination of embryos at embryonic day 16.5 also did not demonstrate any abnormalities. The retinas from adult mice were examined in detail, because neurons are particularly oxidatively active (hence a reflection of mitochondrial function) and because developmental apoptosis is normal in the retina (hence a reflection of apoptosis). Particular attention was given to the numbers of neurons in the ganglion cell layer, the inner nuclear layer, and the outer nuclear cell layer of the retina, and no differences were found between WT and null mice.

Mitochondrial genome structure. Because of the abundance of endo G in the mitochondrial intermembrane space and because R-loops are present at the mitochondrial origin of replication in the mtDNA in the nearby matrix, we examined whether *endo* $G^{-/-}$ mice display changes in the steady-state amount of mtDNA per cell. Total cellular DNA was purified from mouse liver tissue and digested with NsiI, EcoRV, or BglII/EcoRI. Digests were electrophoresed through a 0.8% LE agarose gel and Southern blotted. The membrane was probed with a mixture of three EcoRV-digested, ^{32}P-labeled plasmids, MumX-1.9, -5.1, and -7.6, each of which contains a unique XbaI fragment of murine mtDNA (Fig. 3). We found no difference in the amount of total mtDNA per cell (Fig. 3). The Southern blot analysis also reveals that there is no consistent alteration in mtDNA structure (Fig. 3). We were careful to note any smearing of any of the mtDNA bands in the *endo* $G^{-/-}$ mice that might indicate that random deletions were causing variation in size of some regions of the mtDNA. We saw no evidence of such variation upon overexposure of the gels. These experiments were done on *endo* $G^{-/-}$ mice from the second and third breeding generations to test for any accumulated impact of the lack of endo G over several generations, and we saw no differences. We conclude that endo G does not affect overall mammalian mtDNA metabolism.

Mitochondrial genome sequence. Although we saw no mtDNA structural abnormalities in the *endo* $G^{-/-}$ mice, we considered whether DNA sequence changes might be found. To purify mtDNA for sequencing, a modified version of the protocol was used (16). For each clone, 350 bp was sequenced from the D-loop through the CSBs to the light-strand pro-

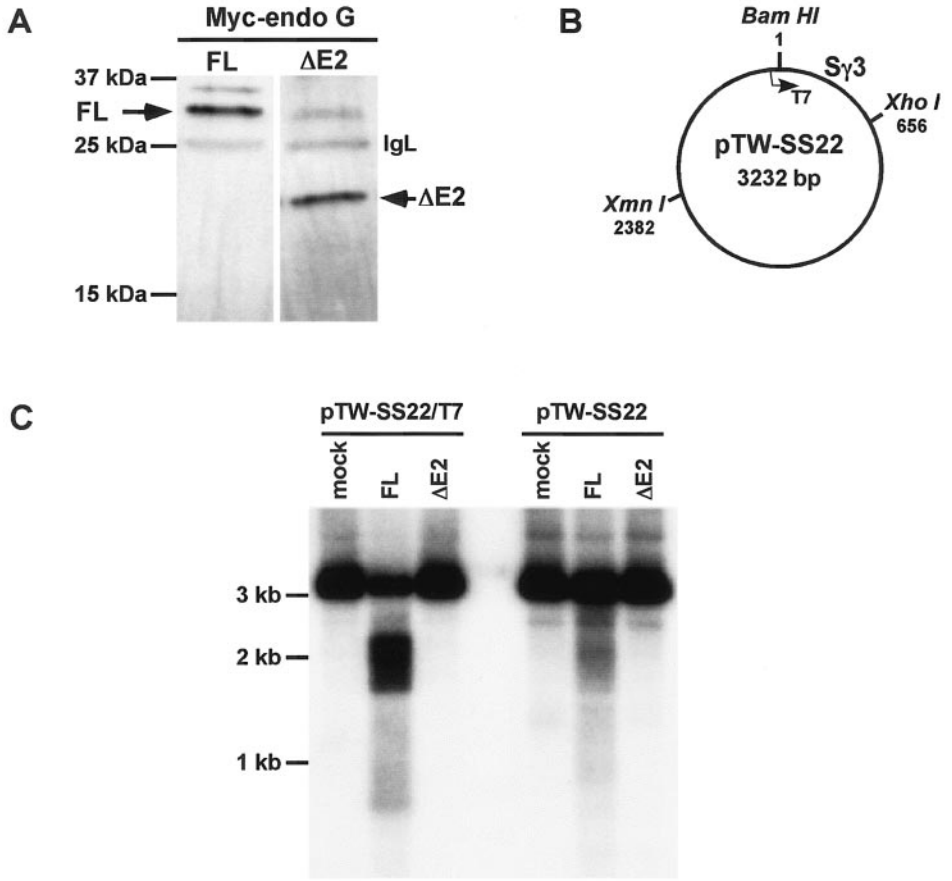

FIG. 2. Recombinant forms of the wild-type and mutant forms of the endo G protein and nuclease activity assays. A. Recombinant forms of the myc epitope-tagged mature endo G and the predicted truncated form (120 aa from exon 1 plus 3 aa from exon 3) of endo G with a 21-aa his-myc C-terminal epitope tag (used for purification). Expression vectors indicated at the top of each lane were transfected into 293 cells, and the proteins were purified with anti-myc immunobeads (see Materials and Methods). The full-length (FL) recombinant mature form migrates at the expected position of 30 kDa (250 aa for the mature form plus 21 aa for the his-myc tag), as seen on this Western blot (arrow). The truncated (ΔE2 for exon 2 deleted) recombinant form is expected to migrate at 21 kDa (167 aa plus the 21-aa his-myc tag) before processing and 16 kDa (123 aa plus the 21-aa his-myc tag) after processing (arrow). The truncated processed form (16 kDa) migrates at a slightly slower position than expected (~19 kDa). The immunoglobulin light chain (IgL) band is indicated. There is a cross-reactive band above the IgL band in the ΔE2 lane, which may represent a proteolytic fragment of the c-*myc* protein. The cross-reactive band in the FL lane at 35 kDa is a cross-reactive band of unknown identity. B. Substrate for assay of nuclease activity of the wild-type and truncated forms of endo G. R-loops were generated using T7 RNA polymerase transcription through a murine immunoglobulin class switch region as described previously. The switch region is located between positions 1 and 656 bp on the plasmid, pTW-SS22. C. Nuclease assay of the wild-type and truncated forms of endo G. The recombinant full-length (FL) endo G or the truncated form of the protein were incubated with the T7 RNA polymerase-transcribed pTW-SS22 plasmid (R-loop conformation of the substrate) (left gel) or with nontranscribed pTW-SS22 (right gel). The pTW-SS22 plasmid was linearized at XmnI. Breaks due to endo G anywhere within the R-loop switch region generated a distribution of linear products between 1,726 and 2,382 bp and another distribution between 850 and 1,506 bp, as seen in the FL lane of the left gel. Overexposure of this gel showed absolutely no evidence of R-loop cleavage activity in the ΔE2 lane of the left gel, and the intact full-length linearized plasmid band in the ΔE2 lane indicates that endo G has no nicking or dsDNA nuclease activity on duplex DNA. In the right gel, full-length recombinant endo G does have a small amount of nicking activity (relative to activity on the R-loop) on duplex supercoiled DNA, as described previously (7, 8, 10, 11, 17).

moter LSP (corresponding to nt 15862 to 16212 [2]). Mutations were identified as deviations from the mouse L-cell mtDNA sequence (2). We noted insertions, deletions, and point mutations (transitions and transversions). We found no significant difference in the mutation rate (Table 2). We conclude that endo G does not affect the mtDNA sequence.

DNA fragmentation and chromatin condensation apoptosis analyses. Because endo G has been shown to participate in *C. elegans* apoptosis, we tested for changes in apoptosis in murine B cells. Splenocytes were prepared (29) from 10- to 12-week-old WT and KO mice and resuspended in RPMI 1640 containing 10% FBS and 50 μM 2-mercaptoethanol alone or this medium with 50 μM etoposide or 500 nM actinomycin D to a density of 5×10^5 cells/ml. For each treatment, 6×10^6 cells were transferred to a single 10-cm-diameter dish and incubated for 12 h at 37°C and 5% CO_2. Genomic DNA was purified from 5×10^6 cells and dissolved in 30 μl of TE, and the DNA in 2 μl of each DNA sample was resolved on an agarose gel (Fig. 4A). We saw no difference in DNA fragmentation from cells undergoing apoptosis due to either etoposide or actinomycin D.

To visualize nuclear chromatin condensation, 10^6 cells were

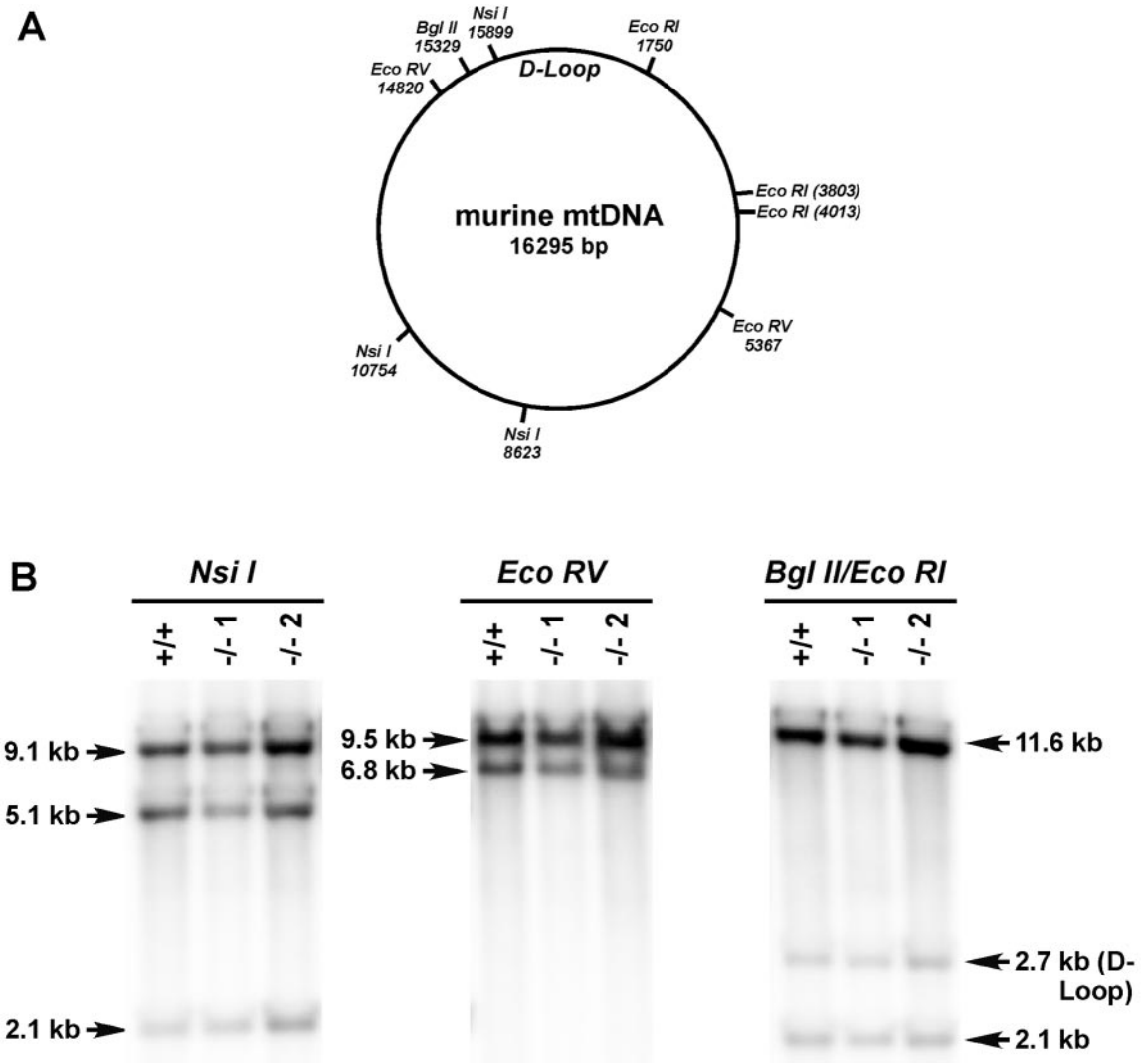

FIG. 3. Mitochondrial genome copy number and gross structure. A. Diagram of the murine mitochondrial genome. The D-loop region of the mitochondrial genome is shown along with restriction sites. B. Southern blots of the murine mitochondrial genome. Fragments (see Materials and Methods) from the murine mitochondrial genome were used as probes on restricted mtDNA harvested from equivalent amounts of liver DNA from wild-type (+/+) and two *endo* $G^{-/-}$ (−/−) mice. No differences in intensity, sizes of specific bands, or variations in the distribution of DNA (smearing) around each band were noted as this or darker exposures.

fixed and stained with DAPI and examined by fluorescence microscopy (Fig. 4B and C). We saw no difference in the frequency or cytological characteristics of the nuclear condensation and fragmentation in the *endo* $G^{-/-}$ mice relative to wild-type mice. We infer from these studies that the absence of endo G does not have a major impact on these apoptosis DNA fragmentation rates or characteristics.

DISCUSSION

endo G is not essential for viability. Here we have deleted exon 2 of the *endo G* gene, which causes exon 3 to be out of frame, when spliced to exon 1. We do not think that the putative truncated protein is produced from the disrupted allele on the basis of the results of Western blot analysis. However, if such a truncated protein were produced, it would correspond to the first exon plus three amino acids encoded by

TABLE 2. Summary of murine mtDNA control region sequencing

Characteristic	Mice	
	endo $G^{+/+}$	*endo* $G^{-/-}$
No. of clones sequenced	68	79
Total bases sequenced	23,800	27,650
Clones with at least 1 mutation (%)	19 (28)	21 (27)
Total no. of mutations	26	28
Transitions[a]	19	26
Transversions[b]	4	1
Deletions[c]	2	1
Insertions[d]	1	0
Mutation rate	1.1E − 3[e]	1.0E − 3

[a] C to T, T to C, A to G, or G to A.
[b] C or T changed to A or G.
[c] Single-nucleotide deletions.
[d] Single-nucleotide insertions.
[e] 1.1E − 3, 1.1×10^{-3}.

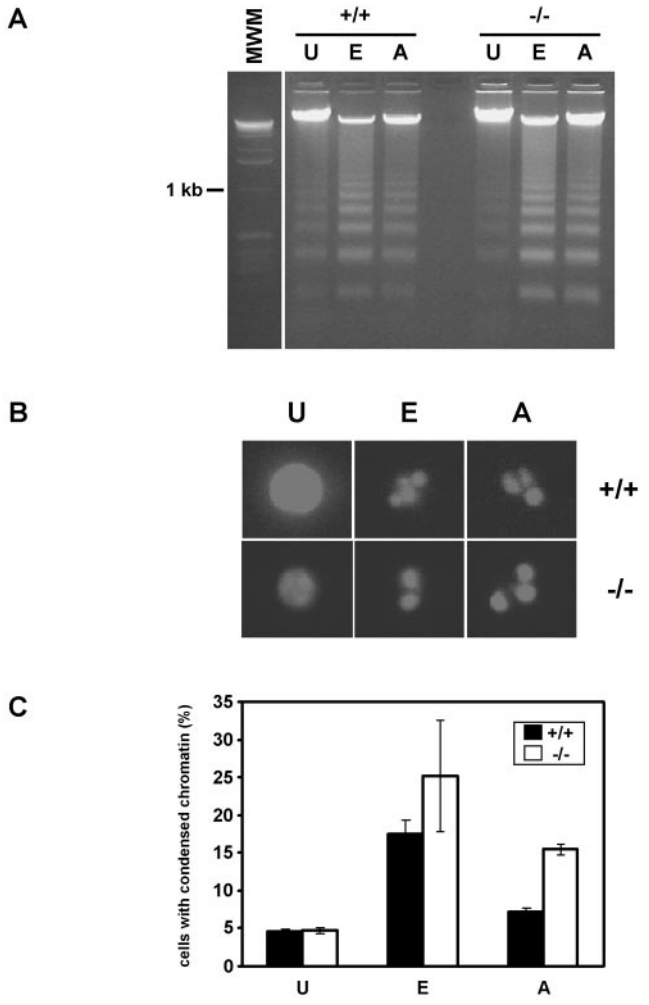

FIG. 4. Apoptosis assays on cells from wild-type (+/+) or *endo* $G^{-/-}$ (−/−) mice. A. DNA laddering in DNA from untreated (U) cells or cells treated with etoposide (E) or actinomycin D (A). Isolated splenocytes were resuspended in RPMI 1640 containing 10% FBS and 50 μM 2-mercaptoethanol with no additional treatment (U) or with 50 μM etoposide (E) or 500 nM actinomycin D (D) to a density of 0.5×10^6 cells/ml. For each treatment, 12 ml of cells (6×10^6 cells) were transferred to a single 10-cm-diameter dish and incubated for 12 h at 37°C and 5% CO_2. Genomic DNA was purified from 5×10^6 cells, dissolved in 30 μl of TE, and resolved on a 1.5% LE agarose gel. The positions of molecular size standards (MWM) (in kilobases) are indicated to the left of the gels. B. Nuclear fragmentation assay. Cells (10^6 cells) from the same dishes were fixed in 3.7% formaldehyde and stained with DAPI (see Materials and Methods). A minimum of 200 nuclei were analyzed for chromatin condensation by fluorescence microscopy per treatment arm of the experiment. C. Quantitation of nuclear fragmentation assay. Histograms of the data derived from panel B.

exon 3. We specifically created the recombinant form of the putative truncated protein and compared it to the full-length protein and detected no nuclease activity. If it has activity, it is reduced at least 100-fold from that of the mature full-length endo G protein.

Why did we not delete all three exons of the *endo G* gene? We certainly would have done this if it were feasible. However, repetitive DNA located immediately upstream and downstream of the gene precludes this. More importantly, there is a 10-exon gene, D2Wsu81e, located immediately adjacent to the *endo G* gene and positioned in a tail-to-tail orientation. The tenth exon of this gene actually overlaps with the third exon and part of the second intron of the *endo G* gene (Fig. 1A). This conserved ORF encodes a predicted protein with a conserved DNA binding domain. The mRNA for this gene is expressed at high levels in blastocysts and at even higher levels at embryonic day 6.5 to 9.5 (http://genome.cse.ucsc.edu). This may explain why its alteration might lead to early embryonic lethality (28). Close proximity of about 20% of human genes, particularly ones oriented in a head-to-head configuration with a bidirectional promoter region, was described recently, making this an important complication in genetic disruption studies (1). Subsequently, others have confirmed the close proximity of such a subset of mammalian genes (21, 22).

After we had completed the laboratory work for this study and were preparing it for publication, another group published a study attempting an *endo G* knockout (28). Unnoted in their study is the existence of the adjacent and overlapping tail-to-tail gene, D2Wsu81e. They deleted nearly all of the *endo G* gene, but they also deleted 5 of the 10 exons of the adjacent gene. Our disruption does not affect the third exon of *endo G* (which overlaps the tenth exon of D2Wsu81e) or any of the exons of the D2Wsu81e gene.

There is a major difference in phenotype between our *endo G* disruption and the inadvertent double-gene disruption described by others (28). Even their heterozygous mice show abnormalities. Their homozygous mice die during embryogenesis at day 3. Our *endo* $G^{-/-}$ mice are viable and have no obvious phenotype even at 1 year of age. Because our disruption results in no apparent endo G expression (>100-fold reduction, if any at all) and because any residual protein has lost its nuclease activity, it is hard to imagine that our study is confounded by any residual, but unmeasurable, endo G activity. Such a possibility seems even less likely given that the other study described a phenotype with merely a 50% reduction in expression (the heterozygote). We believe that the other study is complicated by effects on the adjacent partially deleted gene and that the true *endo G* null mutation is as described here. Our study is more in line with the corresponding null mutations in *S. cerevisiae* and in *C. elegans* (18), where the *endo G* null mutation is not at all lethal. Not only is the *endo G* null mutation in *C. elegans* viable, but the effect on apoptosis, while detectable, is not particularly large (18).

endo G and mtDNA. The absence of endo G did not influence mtDNA copy number, structure, or mutation rate. Hence, endo G may play no critical role in mtDNA metabolism. This is also consistent with the findings observed with *S. cerevisiae* (27). This suggests that the inner mitochondrial membrane serves as an effective barrier between endo G in the intermembrane space and the mtDNA in the matrix.

endo G has been suggested to be part of an ancient family of DNA or RNA nonspecific nucleases (20). The prokaryotic members of this family are usually secreted, perhaps to degrade local decaying biological material to then serve as a nutritional source. With the evolution of mitochondria as intracellular symbiotes within eukaryotes, these secreted proteins may have remained within the intermembrane space.

Hence, there is not necessarily a mitochondrial role for such an enzyme. Its location could simply be an evolutionary vestige.

endo G and apoptosis. It would have been tempting to think that the mitochondrial location of endo G is ideal for release during cell death. However, none of the *endo G* null mutations (in *S. cerevisiae*, *C. elegans*, or mice [as described here]) provide compelling evidence of large effects on apoptosis (18, 27). All of the effects on apoptosis are either small or nonexistent. Even those who advocate a role in apoptosis acknowledge that the effects are quite small compared to the other nuclease of apoptosis, DFF (or CAD) (18, 28). The effect of a clean-up nuclease on the number of extra cells during *C. elegans* development is small, and such a connection requires complex explanations.

Apoptosis inhibitory factor (AIF) is also a mitochondrial intermembrane protein that is released during apoptosis. Mice with a retroviral interruption of *aif* lack AIF activity (12). Such mice have a phenotype that is most obvious in neuronal tissues. When *endo* $G^{-/-}$ mice were crossed with *aif*$^{-/-}$ mice, the phenotype was the same as that for the *aif*$^{-/-}$ mice, and no additional phenotypes could be identified (R. Irvine and M. R. Lieber, data not shown).

endo G and other possible functions. Why would a highly conserved nuclease that is located in the mitochondrial intermembrane space have a phenotype that is so minimal that it escapes the analysis done here? We do not know. Although we have analyzed these mice for more than five generations, we cannot rule out the possibility that future generations will show some sort of accumulated impact on the mitochondrial genome. Alternatively, perhaps endo G is involved in apoptotic DNA removal, but the effects are too small to be measured by the assays used here.

Alternatively, could endo G have other nuclease functions not yet tested for? Our interest in endo G stems from an interest in identifying R-loop cleavage activities related to immunoglobulin class switch recombination. The immunoglobulin heavy-chain isotype levels in blood were not different in wild-type or heterozygous mice (see Fig. S1 in the supplemental material). Hence, we have ruled out the hypothesis that endo G is involved in class switch recombination. However, other nuclease functions of some nonessential nature are conceivable. Until a specific assay is used to test these mice, the precise function of endo G continues to remain unclear.

ACKNOWLEDGMENTS

We thank Adolf Ruiz-Carrillo for considerable help in initial understanding of the *endo G* locus. We thank Michael Koss for help in interpreting the liver cell electron microscopy. We thank G. Attardi and Ann Chomyn for reagents and advice on the mtDNA analyses.

This work was supported in part by NIH grants.

REFERENCES

1. **Adachi, N., and M. R. Lieber.** 2002. Bidirectional gene organization: a common architectural motif of the human genome. Cell **109:**807–809.
2. **Bibb, M. J., R. A. van Etten, C. T. Wright, M. W. Walberg, and D. A. Clayton.** 1981. Sequence and gene organization of mouse mitochondrial DNA. Cell **26:**167–180.
3. **Cerritelli, S. M., E. G. Frolova, C. Feng, A. Grinberg, P. E. Love, and R. J. Crouch.** 2003. Failure to produce mitochondrial DNA results in embryonic lethality in Rnaseh1 null mice. Mol. Cell **11:**807–815.
4. **Chang, D. D., W. W. Hauswirth, and D. A. Clayton.** 1985. Replication priming and transcription initiate from precisely the same site in mouse mitochondrial DNA. EMBO J. **4:**1559–1567.
5. **Clayton, D. A.** 1991. Replication and transcription of vertebrate mitochondrial DNA. Annu. Rev. Cell Biol. **7:**453–478.
6. **Clayton, D. A.** 1992. Transcription and replication of animal mitochondrial DNAs. Int. Rev. Cytol. **141:**217–232.
7. **Côté, J., J. Renaud, and A. Ruiz-Carrillo.** 1989. Recognition of (dG)n/(dC)n sequences by endonuclease G. J. Biol. Chem. **264:**3301–3310.
8. **Côté, J., and A. Ruiz-Carrillo.** 1993. Primers for mitochondrial DNA replication generated by endonuclease G. Science **261:**765–769.
9. **Daniels, G. A., and M. R. Lieber.** 1995. RNA:DNA complex formation upon transcription of immunoglobulin switch regions: implications for the mechanism and regulation of class switch recombination. Nucleic Acids Res. **23:**5006–5011.
10. **Gerschenson, M., K. L. Houmiel, and R. L. Low.** 1995. Endonuclease G from mammalian nuclei is identical to the major endonuclease of mitochondria. Nucleic Acids Res. **23:**88–97.

10a. **Hsieh, C. L.** 1994. The dependence of transcriptional repression on CpG methylation density. Mol. Cell. Biol. **14:**5487–5494.

11. **Huang, K. J., B. V. Zemelman, and I. R. Lehman.** 2002. Endonuclease G, a candidate human enzyme for the initiation of genomic inversion in herpes simplex type 1 virus. J. Biol. Chem. **277:**21071–21079.
12. **Klein, J. A., C. M. Longo-Guess, M. P. Rossman, K. Seburn, R. Hurd, W. Frankel, R. T. Bronson, and S. L. Ackerman.** 2002. The harlequin mouse mutation down-regulates apoptosis-inducing factor. Nature **419:**367–374.
13. **Lee, D. Y., and D. A. Clayton.** 1998. Initiation of mitochondrial DNA replication by transcription and R-loop processing. J. Biol. Chem. **273:**30614–30621.
14. **Lee, D. Y., and D. A. Clayton.** 1996. Properties of a primer RNA-DNA hybrid at the mouse mitochondrial DNA leading-strand origin of replication. J. Biol. Chem. **271:**24262–24269.
15. **Li, L. Y., X. Luo, and X. Wang.** 2001. Endonuclease G is an apoptotic DNase when released from mitochondria. Nature **412:**95–99.
16. **Michikawa, Y., and G. Attardi.** 2002. Screening for aging-dependent point mutations in mtDNA. Methods Mol. Biol. **197:**75–92.
17. **Ohsato, T., N. Ishihara, T. Muta, S. Umeda, S. Ikeda, K. Mihara, N. Hamasaki, and D. Kang.** 2002. Mammalian mitochondrial endonuclease G. Eur. J. Biochem. **269:**5765–5770.
18. **Parrish, J., L. Li, K. Klotz, D. Ledwich, X. Wang, and D. Xue.** 2001. Mitochondrial endonuclease G is important for apoptosis in *C. elegans*. Nature **412:**90–94.
19. **Prats, E., M. Noel, J. Letourneau, V. Tiranti, J. Vaque, R. Debon, M. Zeviani, L. Cornudella, and A. Ruiz-Carrillo.** 1997. Characterization and expression of the mouse endonuclease G gene. DNA Cell Biol. **16:**1111–1122.
20. **Schafer, P., S. R. Scholz, O. Gimadutdinow, I. A. Cymerman, J. Bujnicki, A. Ruiz-Carrillo, A. Pingoud, and G. Meiss.** 2004. Structural and functional characterization of mitochondrial EndoG, a sugar non-specific nuclease which plays an important role during apoptosis. J. Mol. Biol. **338:**217–228.
21. **Takai, D., and P. A. Jones.** 2004. Origins of bidirectional promoters: computational analysis of intergenic distance in the human genome. Mol. Biol. Evol. **21:**463–467.
22. **Trinklein, N., S. F. Aldred, S. Hartman, D. Schroeder, R. Otillar, and R. M. Myers.** 2004. An abundance of bidirectional promoters in the human genome. Genome Res. **14:**62–66.
23. **Xu, B., and D. A. Clayton.** 1995. A persistent RNA-DNA hybrid is formed during transcription at a phylogenetically conserved mitochondrial DNA sequence. Mol. Cell. Biol. **15:**580–589.
24. **Xu, B., and D. A. Clayton.** 1996. RNA-DNA hybrid formation at the human mitochondrial heavy-strand origin ceases at replication start sites: an implication for RNA-DNA hybrids serving at primers. EMBO J. **15:**3135–3143.
25. **Yu, K., F. Chedin, C.-L. Hsieh, T. E. Wilson, and M. R. Lieber.** 2003. R-loops at immunoglobulin class switch regions in the chromosomes of stimulated B cells. Nat. Immunol. **4:**442–451.
26. **Yu, K., and M. R. Lieber.** 2003. Nucleic acid structures and enzymes in the immunoglobulin class switch recombination mechanism. DNA Repair **2:**1163–1174.
27. **Zassenhaus, H. P., and G. Denniger.** 1994. Analysis of the role of the NUC1 endo/exonuclease in yeast mitochondrial DNA recombination. Curr. Genet. **25:**142–149.
28. **Zhang, J., M. Dong, L. Li, Y. Fan, P. Pathre, J. Dong, D. Lou, J. M. Wells, D. Olivares-Villagomez, L. Van Kaer, X. Wang, and M. Xu.** 2003. Endonuclease G is required for early embryogenesis and normal apoptosis in mice. Proc. Natl. Acad. Sci. USA **100:**15782–15787.
29. **Zhang, J., X. Liu, D. C. Scherer, L. Van Kaer, X. Wang, and M. Xu.** 1998. Resistance to DNA fragmentation and chromatin condensation in mice lacking the DNA fragmentation factor 45. Proc. Natl. Acad. Sci. USA **95:**12480–12485.